Production of High-Order Micromachined Silicon Echelles on Optically Flat Substrates

Oleg A. Ershov[a], Daniel T Jaffe[a], Jasmina P. Marsh[a], Luke D. Keller[b]

[a]Dept. of Astronomy, Univ. of Texas, Austin, TX 78712, USA

[b]Center for Radiophysics and Space Research, Cornell Univ., Ithaca, NY 14853, USA

ABSTRACT

Infrared spectrometers using silicon immersion gratings and grisms can have substantial performance advantages over conventional instruments. The immersion gratings and grisms share a common geometry: prism-shaped pieces of silicon with blazed grooves along one side. The grooves can either be machined directly into substrates or the grooves can be machined into thin wafers which are then bonded to flat-surfaced prisms. Chemical micromachining currently is the best method of "ruling" grooves directly into silicon surfaces. The tolerances for near-IR diffraction gratings make direct machining of the grooves onto one surface of a bulky, prism-shaped substrate very difficult. We encountered a number of issues that we had to resolve when we tried to etch precisely positioned grooves into massive pieces of silicon: silicon substrate purity, lithography mask alignment, photoresist thickness uniformity, temperature control, wet etching vs. reactive-ion etching. We have successfully manufactured 7 line / mm gratings on 15 mm thick substrates. We performed optical tests with these gratings used as front-surface devices to determine efficiency and diffraction limited performance. Our echelle gratings have 70% efficiency in $365^{\rm th}$-$368^{\rm th}$ order at 632.8 nm. Testing shows that the grating preserves a diffraction-limited point-spread function making them good dispersing elements for applications requiring high spectral resolving power.

Keywords: wet etching, echelle, optically flat, diffraction-limited image

1. INTRODUCTION

Silicon immersion gratings and grisms can greatly improve the performance of diffractive infrared spectrometers. The high refractive index of Si is responsible for most of this improvement. In grism instruments, where the resolving power scales with n-1 (where n is the refractive index, $\sim$3.44 for Si in the near-IR), instruments can have collimated beam sizes 2-3 times smaller at a given resolving power using Si as opposed to other common IR optical materials. Immersion grating spectrometers can have beam sizes n times smaller than those of instruments with conventional front-surface diffraction gratings. Since the volume of spectroscopic instruments tends to scale with the square or cube of the collimated beam size, these smaller beams can translate into very substantial reductions in size and weight.

The critical dimension in a diffraction grating is the spacing from one blazed groove surface to the surface of any other groove. Gratings or grisms where the groove positions deviate from a regular interval do not reflect monochromatic light coherently and rapidly lose diffraction efficiency. Moreover, gratings with deviations of groove positions on large spatial scales cannot produce diffraction limited spectral point spread functions appropriate to the width of the incident beam and the grating angle. For example, to achieve 70% efficiency for a grating used in immersion and grism modes, the allowable RMS deviation in groove spacing[1] is given by

$$\Delta\sigma_{\rm rms} = \frac{0.134\lambda\,(\mu{\rm m})}{2{\rm n}\,\sin\,\delta}\ \mu{\rm m} \quad \text{for an immersion grating} \tag{1}$$

$$\Delta\sigma_{\rm rms} = \frac{0.134\lambda\,(\mu{\rm m})}{({\rm n}-1)\,\sin\,\delta}\ \mu{\rm m} \quad \text{for a grism} \tag{2}$$

Further author information: (Send correspondence to O.A. Ershov; phone: (512) 471-3337, fax: (512) 471-6016)
O.A. Ershov: Email: ershov@astro.as.utexas.edu
D.T. Jaffe: E-mail: dtj@astro.as.utexas.edu
L.D. Keller: E-mail: ldk2@cornell.edu
J.P. Marsh: E-mail: jasna@astro.as.utexas.edu

where δ is the prism opening angle and λ is the wavelength of the light incident on the dispersive device (see Figure 1). The difference between the two expressions comes from the optical path difference which includes a factor of 2n for the immersion mode and a factor of n-1 for the grism mode.

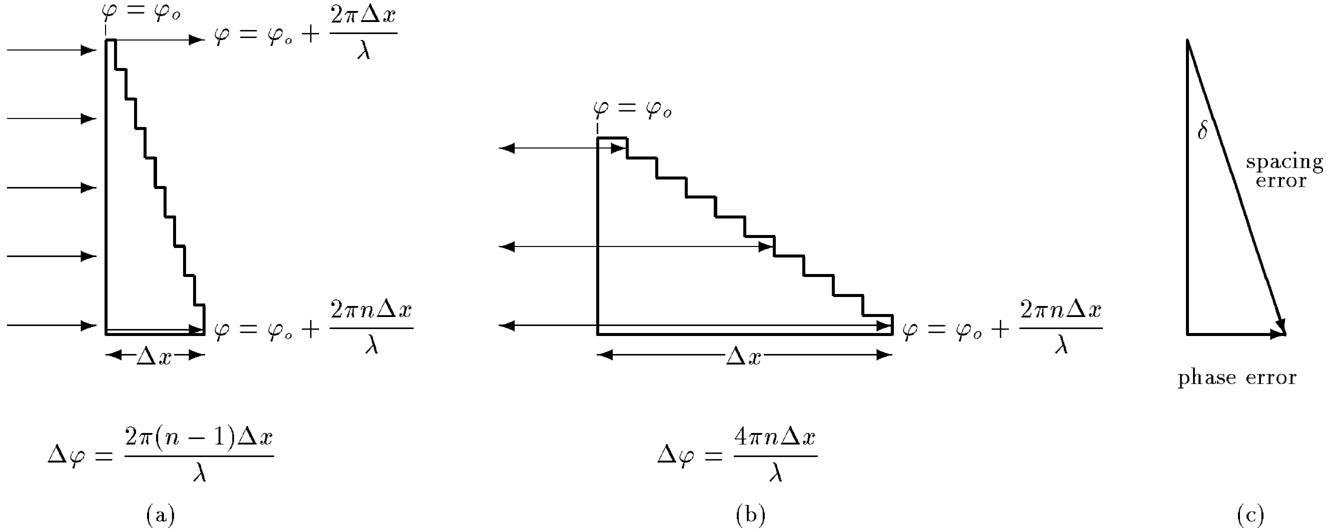

Figure 1. Optical path difference for (a) a grism and (b) and immersion grating. The sin δ term in equations (1) and (2) comes from the projection of the spacing error to the optical path direction shown in part (c).

There are two possible paths to production of prisms with grooved surfaces: direct machining of the grooves into bulk substrates, either before or after appropriate shaping, or machining of the grooves into thin wafers and then bonding the wafers to pre-shaped prisms. Production of diffraction gratings on thin silicon (Si) wafers makes effective use of the existing infrastructure for manufacturing of micromachined parts. Current bonding techniques are capable of optically contacting such wafer gratings to polished prisms to build grisms for use as dispersive elements in astronomical spectrographs[2,3,4]. However, standard commercial wafers are simply not optically flat or of constant thickness. Our recent work and experiments with gratings fabricated on silicon wafers have shown that the final products cannot meet the flatness requirements for efficient performance in the near-IR, particularly when the devices are large (pattern linear dimensions more 30 mm). Variations in the thickness of wafers used as parts of near-IR dispersion elements would lead to distortion of the diffraction wavefront.

In order to avoid the issue of wafer thickness variations, we have elected to produce grooves directly on bulky Si samples. We present here our recent progress in developing fabrication techniques for gratings on thick, optically flat silicon slabs and our efforts to produce efficient silicon gratings for high resolution astronomical spectrographs.[1,5] We have previously produced diffraction gratings on thin wafers and tested the optical performance of these devices. Our best gratings were produced on float-zone silicon with a resistivity of more than 2000 Ω-cm. These devices have up to 80 % efficiency at 632.8 nm (just 6% below theoretical efficiency imposed by our groove geometry when the devices are used as front-surface gratings).[1,5] Because the wafers are not flat, however, these gratings were not diffraction limited on scales larger than a few millimeters. Since we have described our wafer gratings in detail in previous publications,[1,5] we discuss here how the techniques we use to produce gratings on bulky substrates differ from our earlier methods of producing gratings on wafers. We also discuss the results of optical performance tests for the new devices. The primary fabrication issues that have required extra attention are: silicon substrate purity, lithography mask alignment, photoresist thickness uniformity, temperature control with large thermal mass substrates, wet (chemical) etching vs. dry (reactive-ion) etching (RIE) on bulky (large prism-shaped) chunks of silicon.

2. FABRICATION PROCESS

In our initial tests of grating production on bulky substrates, we started with a high purity silicon ingot (resistivity >100 Ω-cm), (100) surface orientation. The ingot was diced into disks of 76 mm diameter and 15 mm thickness. Precise knowledge of the crystal plane orientation is very important to the anisotropic etching process since it allows proper mask alignment. Aligning the mask correctly reduces undercutting of silicon during etching. When using wafers, it was possible to determine the alignment of the crystal planes by scoring the wafer and snapping a small portion off of the edge. Since the thick disks will not fracture in this way, each disk was provided with a flat orientation surface on its edge to define the intersection between (100) and (111) crystal planes to ±0.05 degrees using X-ray crystallography. The crystallographic orientation allows us to avoid the extra step of etching a special splay pattern on part of the (100) surface to provide a guide to mask alignment[6,7]. Once the orientation surfaces have been ground into the edge of the disk, the disk is polished to $\lambda/20$ flatness (at λ=632.8 nm) using a chemical-mechanical planarization (CMP) process. CMP polishing (currently a standard procedure for polishing) avoids damage to the sub-surface crystal lattice by alternating between optical lapping/polishing and chemical etching of the surface.

The next step in grating production is to transfer a pattern of regularly spaced stripes from an unblazed chrome-on-quartz mask/grating to a passivation layer on the polished surface of the silicon disk. In our wafer experiments, we investigated both a SiO_2 and wet etch pattern transfer and a Si_3N_4 plus RIE transfer. The better resistance of the Si_3N_4 passivation layer to undercutting during the anisotropic etching[8,9,10] that follows the patterning resulted in somewhat better quality gratings, particularly when the groove spacings were coarse and the etching times consequently long (a ~5% improvement for 142 μm groove spacing). It is possible to process thick disks using either passivation and patterning technique and we have, therefore passivated disks with both SiO_2 and Si_3N_4. Because we are concerned that RIE machines will not be able to accomodate larger substrates and that odd-shaped dielectric substrates may affect the accuracy with which RIE transfers the pattern, we have elected to do our initial tests using SiO_2 overcoated disks.

In the first patterning step, we overcoat our oriented and polished disks with 600 nm of thermally grown SiO_2. To apply uniform thickness photoresist coatings to our disks, we use a custom-built spin table which can produce the required high angular acceleration (typically up to 4000 RPM in less than 1 second). The spin table draws the required peak angular momentum from a massive steel flywheel that is coupled to the workplace by an electromagnetic clutch. A control loop locks the flywheel speed to a preset value, assuring reproducibility of the coating process and allowing us to vary the angular velocity. We transfer the pattern to the photoresist by contact exposure in a UV illumination system custom built to permit uniform exposure of bulky, odd-shaped substrates.

The large volume of our disks means that they have substantially larger heat capacity and substantially lower surface area to volume ratios than wafer substrates. Cleaning the substrate and hardening the photoresist both require heating the substrate to 100°C. Thin wafers cool from 100°C to 25°C within 1 minute, while the 15 mm thick disks retain heat for at least an hour. Slow substrate cooling after cleaning and baking prior to photoresist coating allows time for contamination by ambient water vapor and particulates. The resist-coated substrate must be baked again before UV-exposure and must be cooled rapidly to prevent photoresist shrinkage and deterioration. To accelerate uniform cooling of thick substrates after each bake step, we placed the hot substrate in contact with a massive aluminum plate at 25°C applying continuous recirculation of air with a jet of 25°C dry nitrogen. Iterating the process, we have established the baking and cooling times which produce the best gratings. Thermal effects are also important during the anisotropic etching which follows patterning of the passivation layer. Etching is done at 60 - 65°C, but in a given etch sequence we regulate the bath temperature to ±0.15°C. To prevent etch rate gradients at the time of immersion, we pre-heat the silicon disks to the bath temperature.

We etch the substrates in an aqueous solution of potassium hydroxide and iso-propanol. Etchant concentration, like temperature, may affect the etch rate and anisotropic etch ratio. We maintain uniform KOH concentration and eliminate local temperature gradients within the bath by providing a recirculating flow of etchant over the disk while producing the grooves. As we did with the wafer substrates, we use ultrasonic agitation to homogenize the etchant bath concentration and to facilitate the detachment of hydrogen bubbles[1,5].

The end result of the fabrication process is a high quality, uniform grating pattern over the entire substrate surface (45 cm^2). The (100) disk surface orientation results in a grating with a symmetric groove profile. We produced an echelle with 142 μm groove spacing and 54.7° blaze angle. Between each groove is a 10 μm wide unblazed stripe, an artifact caused by the finite width of the mask lines (note that these unblazed stripes are invisible when the grating

is used in immersion). The mask was made by Hyperfine, Inc., produced on a quartz substrate with a flatness of $\lambda/20$ (at 632.8 nm).

3. OPTICAL TESTING

The two principal figures of merit for a diffraction grating are the efficiency: what fraction of a monochromatic beam incident on a grating diffracts into a given order and in the desired direction, and the resolution: how wide is the angular spread of the monochromatic dispersed light. We have evaluated performance of our micromachined silicon gratings as front-surface devices, illuminating the grooves from the outsides of the pieces. We present here the results of interferometric measurements of grating accuracy and direct measurements of diffraction efficiency using the devices in a benchtop spectrometer. The effective wavelength of light in a dielectric material is n times shorter than the vacuum wavelength. Consequently, front-surface testing in reflection at a wavelength λ_o/n (~580 nm for λ_o=2 μm) gives a good estimate of an immersion grating performance at λ_o and testing at $2\lambda_o/(n-1)$ (~1.6 μm for λ_o=2 μm) should give results to those obtainable from a grism at $\lambda=\lambda_o$. We analyzed our devices using red (632.8 nm) and green (543.5 nm) HeNe lasers. All tests were made with our interferometer/spectrograph test setup[1] (see Figure 2) described in detail in our previous paper. The setup uses the collimated light from two lasers as light sources. The beam splitter divides the beam between two arms. One arm holds a grating in Littrow configuration and the other holds a reference mirror. The images from the grating and the reference mirror are then combined and focused by a camera lens (f_{camera}=200 mm) onto the CCD (768x512 pixels, 9 μm square pixels).

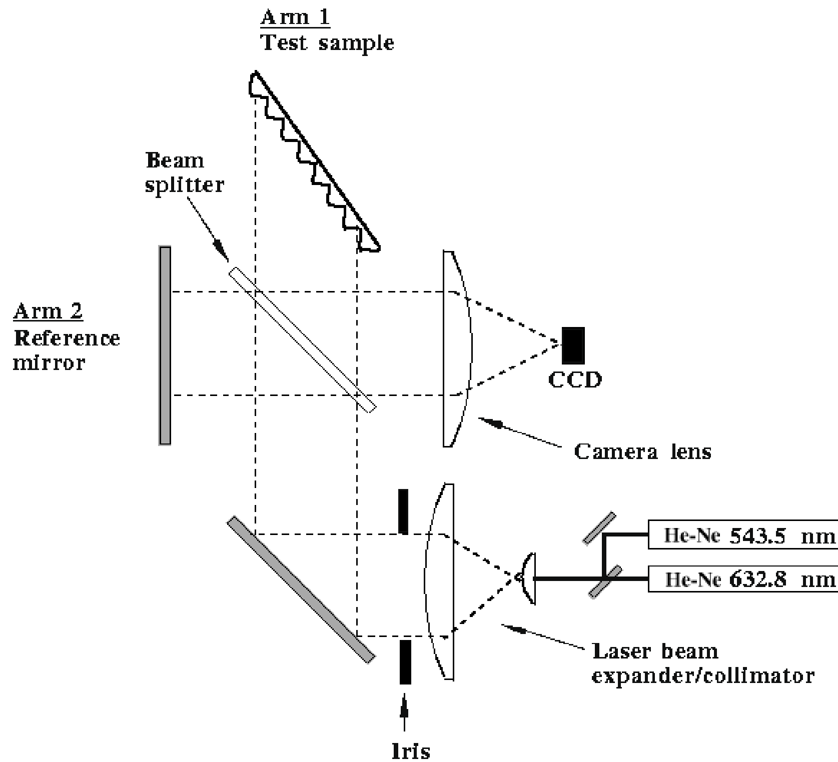

Figure 2. Optical test setup[1] consisting of a dual purpose spectrograph. We use two HeNe lasers as light sources (543.5 nm and 632.8 nm). When used as an interferometer, Arm 2 contains an optical flat. We image the exit pupil to obtain an interferogram and measure the flatness of the sample. When used as a spectrograph, Arm 2 contains a silicon reference mirror which is tilted so the light from it does not interfere with the test beam but still lands on the detector to provide an intensity reference. The camera lens (f_{camera}=200 mm) then images the source onto the CCD (768x512 pixels, 9 μm pixels).

We used the setup as an interferometer to measure the surface flatness of substrates and completed gratings by placing a reference mirror of flatness $\lambda/20$ or better in Arm 2 and imaging the exit pupil produced as this beam interferes with the return beam from the test sample in Arm 1. In Figure 3, we show interferograms obtained (a) for an unetched 15 mm thick disk and (b) for a 15 mm collimated beam illuminating a grating etched subsequently onto the same disk. For the grating, the measured RMS deviation of the fringe positions is 0.085 of the fringe spacing corresponding to an RMS deviation of groove surfaces of 30 nm from the nominal 142 μm spacing.

Figure 3. An interferogram in red light (λ=632.8 nm, collimated beam 20 mm in diameter) of an unetched silicon disk surface (left) and an etched echelle grating in Littrow mode with fringes parallel to grooves (right).

We convert the test setup to spectroscopic mode by tilting the reference flat until the test and reference beams no longer interfere. The reflection from the flat mirror is imaged simultaneously with the spectrum from the grating to provide intensity normalization. In this mode, we use a silicon mirror as the flat in order to factor out the reflectivity of the uncoated diffraction gratings. We used the measured spectra to determine the efficiency at the peak of the blaze by normalizing the diffracted intensity by the intensity of the return beam from the Si flat. For the sample shown in Figure 4, the efficiency was 70 % for red light (orders 365-368) and 65 % for green light (orders 425-428). For the groove geometry as viewed from the front-surface, this efficiency corresponds to an RMS error in groove spacing of 32.3 nm for both green and red light. This result is consistent with the groove spacing error of 30 nm measured from the red interferogram.

Neither wavelength (543.5 nm or 632.8 nm) is the blaze wavelength of our grating. The light is consequently distributed among several orders. In an ideal blazed grating, the distribution of intensities between orders should depend only on the geometric diffraction pattern of the individual grooves. Ruled gratings used in high order often suffer efficiency losses as imperfectly blazed grooves or variations in blaze orientations between grooves distribute power into more orders than in the ideal case. One of the advantages of micromachined gratings is the exquisite flatness and consistent orientation of the groove surfaces. We have predicted the position and width of the intensity function for our gratings based on the *nominal* spacing and width of lines in the original mask, accounting for geometric effects resulting from the blaze angle and illumination of the grating using Equation (3):

$$\mathrm{I(p)} = \left(\frac{\sin \frac{\mathrm{ksp}}{2}}{\frac{\mathrm{ksp}}{2}} \right)^2 \tag{3}$$

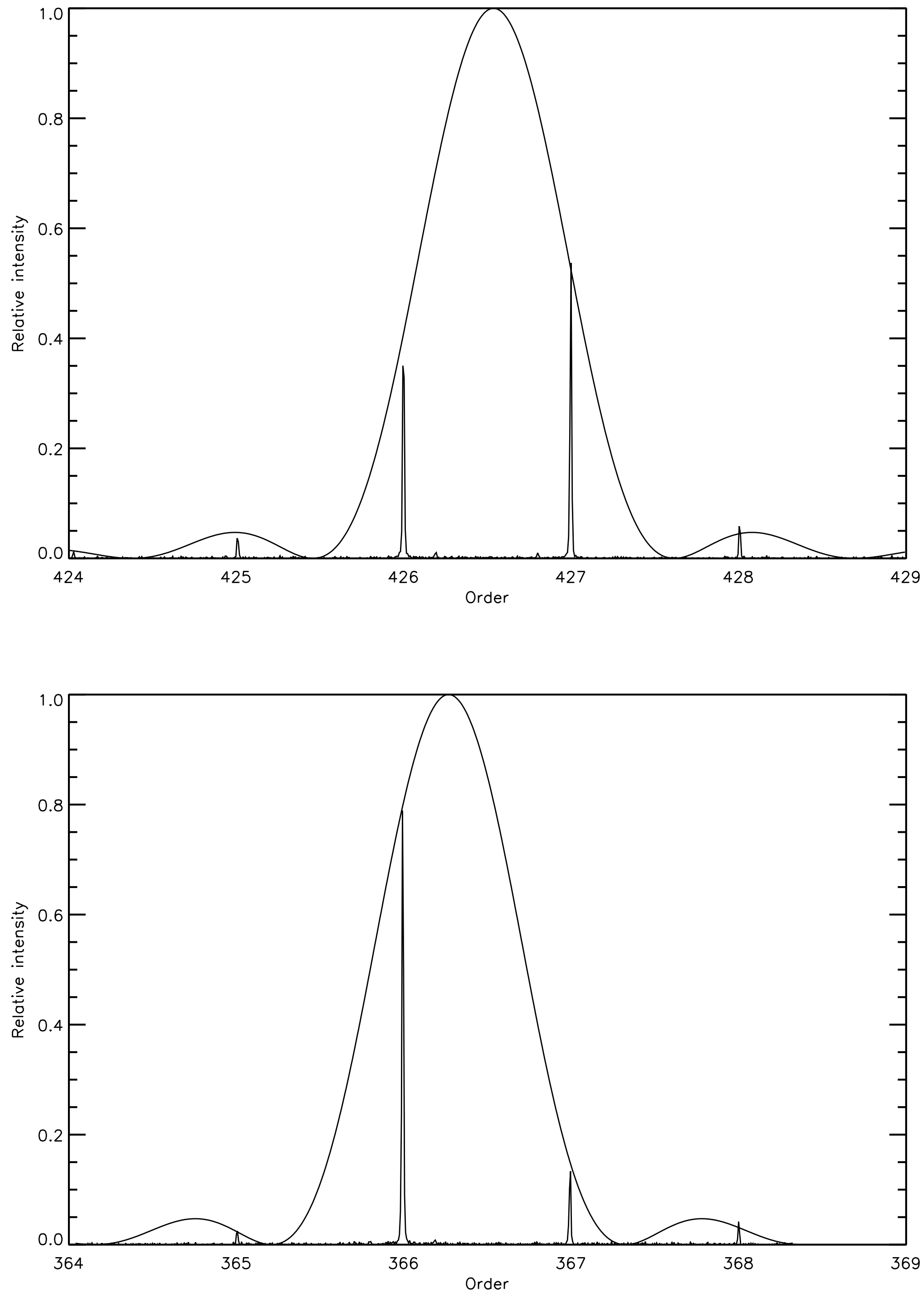

Figure 4. Measured diffraction spectra of the fabricated echelle. Top: λ=543.5 nm, spectral orders of 425-428. Bottom: λ=632.8 nm, spectral orders of 365-368. The groove intensity function is the predicted distribution of power between the observed orders calculated using the effective groove width and spacing and compared to the observed spectrum. No fitting to the observed spectrum was done during this process.

where $k = 2\pi/\lambda$ is the wave number, s is the groove width (76.3 μm), and $p = sin\ \theta - sin\ \theta_0$ where θ_0 is the blaze angle (54.7 degrees in our case) and θ is a variable. Figure 4 shows this calculated intensity distribution superposed on the measured spectra at 543.5 nm and 632.8 nm. No fitting was used to align the calculated and measured distributions. The figure demonstrates graphically that even at 300-400th order, diffraction effects are the primary determinant of the distribution of light between orders.

The irregularities in the groove spacing produced by errors in the placement of the mask lines lower the efficiency of the grating in two different ways. If the errors are random, power lost from the diffracted beam will be distributed throughout the orders containing diffracted power. If the errors are periodic, they will produce "ghosts", small features on either side of spectral lines (e.g. see Figure 4, top). Ghosts visible in the spectra in Figure 4 have a much lower power (around 0.5 % for green light) than we measured in gratings made earlier on wafer substrates.[1]

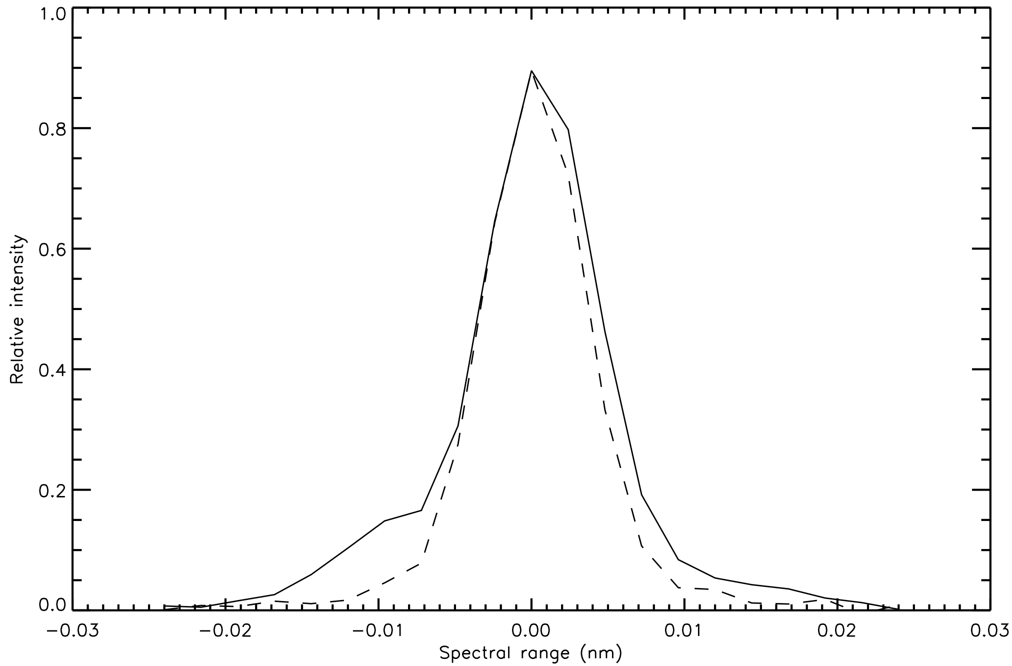

Figure 5. Diffraction-limited performance; illumination at λ=632.8 nm, beam diameter of 20 mm focused by a camera lens with f=838 mm. The diffraction spectral line of the 366th order (solid line) is compared to the instrumental profile (dashed line).

Phase errors on large scales can limit the ultimate resolving power of diffraction gratings. Because the size in the focal plane of a diffraction limited spatial point source is identical to the scale size in the focal plane of the diffraction limited spectral distribution of dispersed light from a monochromatic point source, we can determine the large scale accuracy of our grating by comparing the monochromatic spectral profile to the spatial point-spread function. We placed a long focal length lens in the camera lens position of our spectrograph. A lens with 838 mm focal distance images a 20 mm diameter red light beam to a diffraction-limited spot 32.4 μm (3.6 pixels in a pixel scale), assuming a Gaussian beam profile. Using the 20 mm collimated beam, the diffraction limited resolving power at 632.8 nm is $\lambda/\Delta\lambda$=72,000. The FWHM value of the spectral line we measured for the flat substrate was 3.5 pixels or 0.0084 nm. In fact, Figure 5 shows that at the dispersion of 0.0024 nm/pixel this value closely matches the FWHM of the diffraction-limited spatial profile of our spectrometer. The difference between two measured FWHM values is within experimental errors (0.008 against 0.009 nm); our grating produces diffraction limited point spread function, and we can realize our resolving power requirements. Figure 5 also shows that most of the diffracted power lies within the diffraction limited core of the spectral response function; the Strehl ratio for this grating is 0.83.

4. FUTURE PROGRESS

The device we manufactured on a 76 mm diameter, 15 mm thick disk has been cut and polished into a prism 17 mm tall, 40 mm long and 25 mm wide. We are currently making preparations to test the fabricated echelle in near-IR as a grism and an immersion grating. In both immersion and grism modes, the transmission is different than transmission in the front-surface mode. In the immersion mode, there is no loss from shadowing by the groove tops which accounts for 14 % of light lost in the front-surface mode. In the grism mode, the shadowing becomes even worse due to our grating geometry. Because we are using a prism with a large opening angle as a grism, we will lose 33.2 % of the incident light because of groove geometry. This problem can be avoided by choosing grisms with smaller blaze angles. We expect to produce a batch of different wedges to be used as grisms and immersion gratings. We are also starting to experiment with anti-reflection and reflection coatings for gratings and grisms.

This work was supported by NASA grants NAG5-8858 and NAG5-9230 to the University of Texas at Austin

REFERENCES

1. L. Keller, D. Jaffe, O. Ershov, T. Benedict, U. Graf, "Fabrication and testing of chemically micromachined silicon echelle gratings", *Appl. Optics*, **39**, no.7, pp. 1094-1105, 2000.
2. F. Grey, K. Hermansson, "Preservation of atomically clean silicon surfaces in air by contact bonding", *Appl. Phys. Lett.*,**71**, pp. 3400-3402, 1997.
3. F. Vitali, E. Cianci, D. Lorenzetti, et al. "Silicon grisms for high resolution spectroscopy in the near infrared", *Proc. SPIE*, **4008**, pp. 1383-1394, 2000.
4. H. Käufl, K. Kuhl, S. Vogel, "Grisms from germanium / silicon for astronomical instruments", *Proc. SPIE*, **3354**, pp. 151-158, 1998.
5. D. Jaffe, L. Keller, O. Ershov, "Micromachined silicon diffraction gratings for infrared spectroscopy", *Proc. SPIE*, **3354**, pp. 201-212, 1998.
6. T. Poteat, "Submicron accuracies in anisotropic etched silicon piece parts", in *Micromachining and Micropackaging of Tranducers*, pp. 151-158, edited by C. Fung, Amsterdam, 1985.
7. P. Kuzmenko, D. Ciarlo, "Improving the optical performance of etched silicon gratings", *Proc. SPIE*, **3354**, pp. 357-367, 1998.
8. K. Bean, "Anisotropic etching of silicon", *IEEE Trans. Electron Devices*, **ED-25**, pp. 1185-1193, 1978.
9. H. Seidel, L. Csepregi, A. Kenberger, et al. "Anisotropic etching od silicon in alkaline solutions", *J. Electrochem. Soc.*, **137**, pp. 3612-3626, 1990.
10. D. Kendall, R. Shoultz, "Wet chemical etching of silicon and SiO_2 and ten challenges for micromachiners", in *Handbook of Microlithography, Micromachining and Microfabrication*, pp. 57-97, edited by P. Rai-Choudhury, SPIE Press, 1997.
11. W. Tsang, S. Wang, "Preferentially etched diffraction gratings in silicon", *J. Appl. Phys.*, **46**, pp. 2163-2166, 1975.